Modelling fires in the terrestrial carbon balance by incorporating SPITFIRE into the global vegetation model ORCHIDEE: Part 1. Simulating historical global burned area and fire regime

C. Yue[1], P. Ciais[1], P. Cadule[1], K. Thonicke[2], S. Archibald[3,4], B. Poulter[5], W.M. Hao[6], S. Hantson[7], F. Mouillot[8], P. Friedlingstein[9], F. Maignan[1], N. Viovy[1]

[1]Laboratoire des Sciences du Climat et de l'Environnement, LSCE CEA CNRS UVSQ, 91191 Gif Sur Yvette, France

[2]Potsdam Institute for Climate Impact Research (PIK) e.V., Telegraphenberg A31, 14473 Potsdam, Germany

[3]CSIR Natural Resources and Environment, P.O. Box 395, Pretoria 0001, South Africa

[4]School of Animal, Plant and Environmental Sciences, University of the Witwatersrand, Johannesburg, Private Bag X3,WITS, 2050, South Africa

[5]Institute on Ecosystems and Department of Ecology, Montana State University, Bozeman, MT 59717, USA

[6]US Forest Service, Rocky Mountain Research Station, Fire Sciences Laboratory, Missoula, MT, USA

[7]University of Alcalá, Department of Geography, Calle Colegios 2, Alcalá de Henares 28801, Spain

[8]IRD, UMR CEFE, 1919 route de mende, 34293 Montpellier Cedex 5, France

[9]College of Engineering, Mathematics and Physical Sciences, University of Exeter, EX4 4QE, UK

Supplement

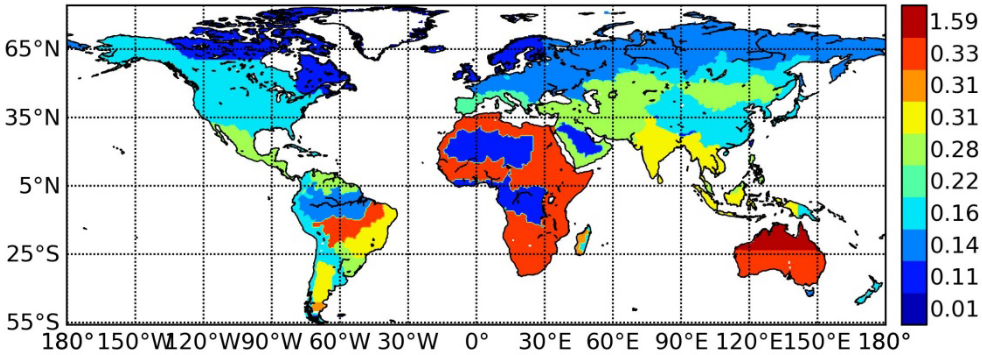

Fig. S1 The spatial distribution of a(ND) (in unit of ignitions ind^{-1} day^{-1}) as used in the human potential ignition equation (Eq. 1 in the main text) by Thonicke et al. (2010).

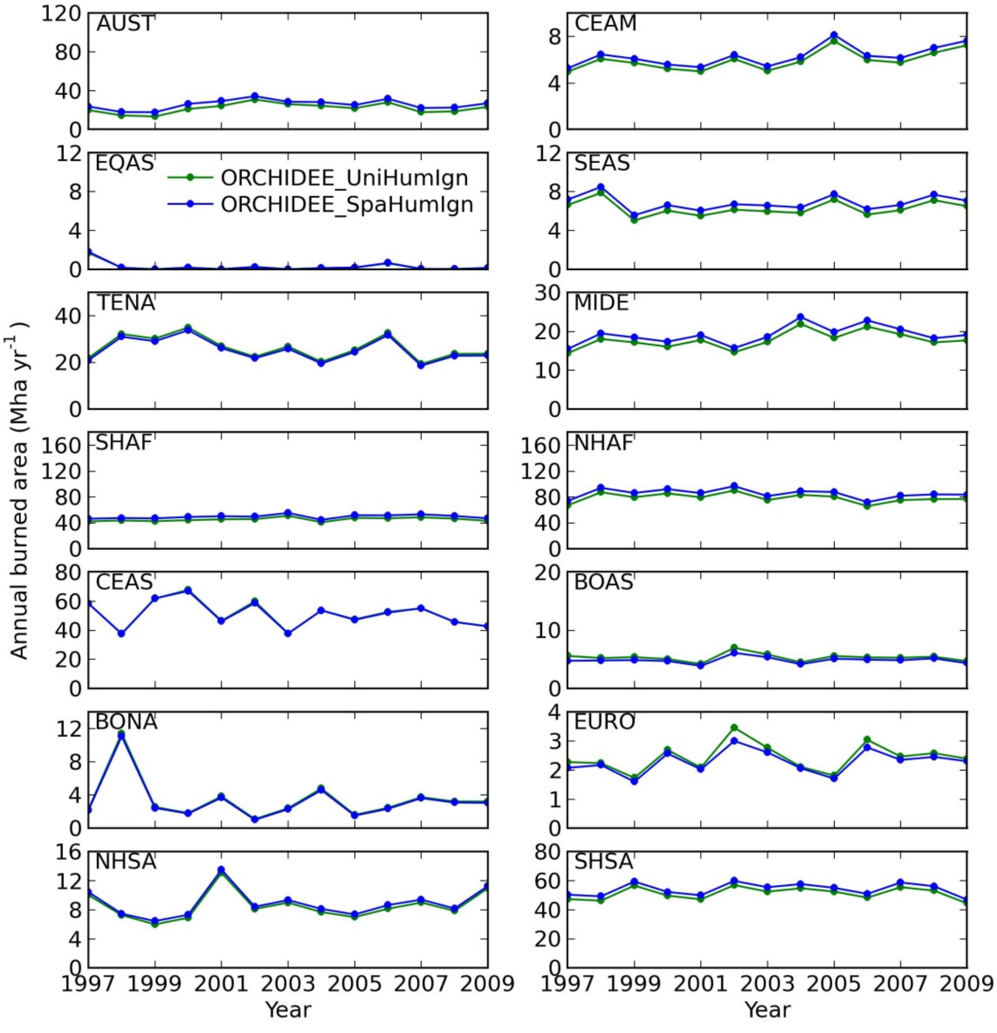

Fig. S2 Simulated annual burned area (1997–2009) for the 14 different GFED3.1 regions by using the a(ND) value of 0.22 (green curve) and by adopting the spatial dataset as shown in Fig. S1 (blue curve). The difference in the annual burned area by the two different parameterizations is rather small. This is mainly because the ignition numbers, as calculated by including a(ND), are only "potential" ignition numbers and they are further scaled by the fire danger index and limited by the ignition efficiency in the model to become "realized" ignitions. Thus the ultimate sensitivity of burned area to this parameter could be small and highly dependent on the fire climate and fuel state.

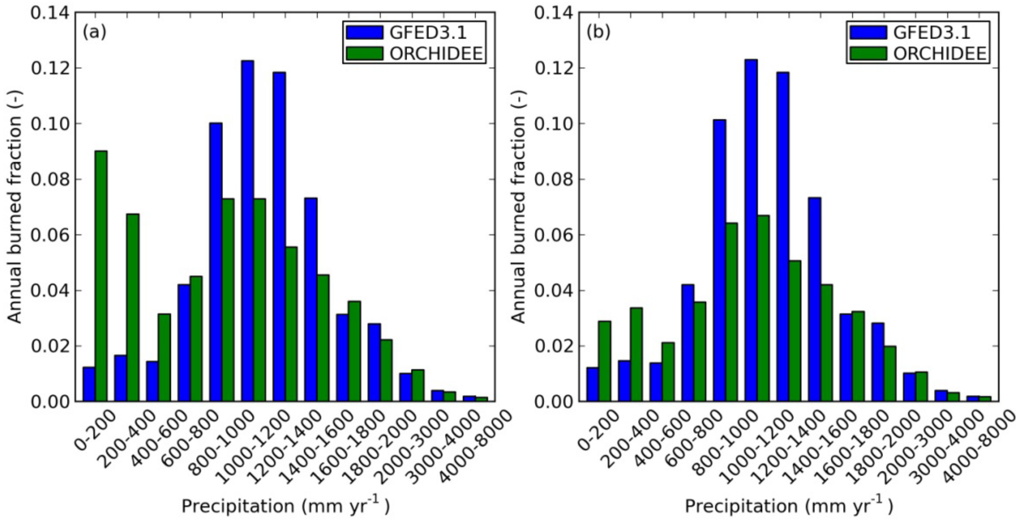

Fig. S3 Mean burned fraction over the precipitation gradient by model simulation and GFED3.1 data for (a) before and (b) after the adoption of fuel load limitation on the ignition efficiency. Burned fraction is averaged over 200-mm precipitation bins and data presented include all the pixels over the globe with burned fraction bigger than zero.

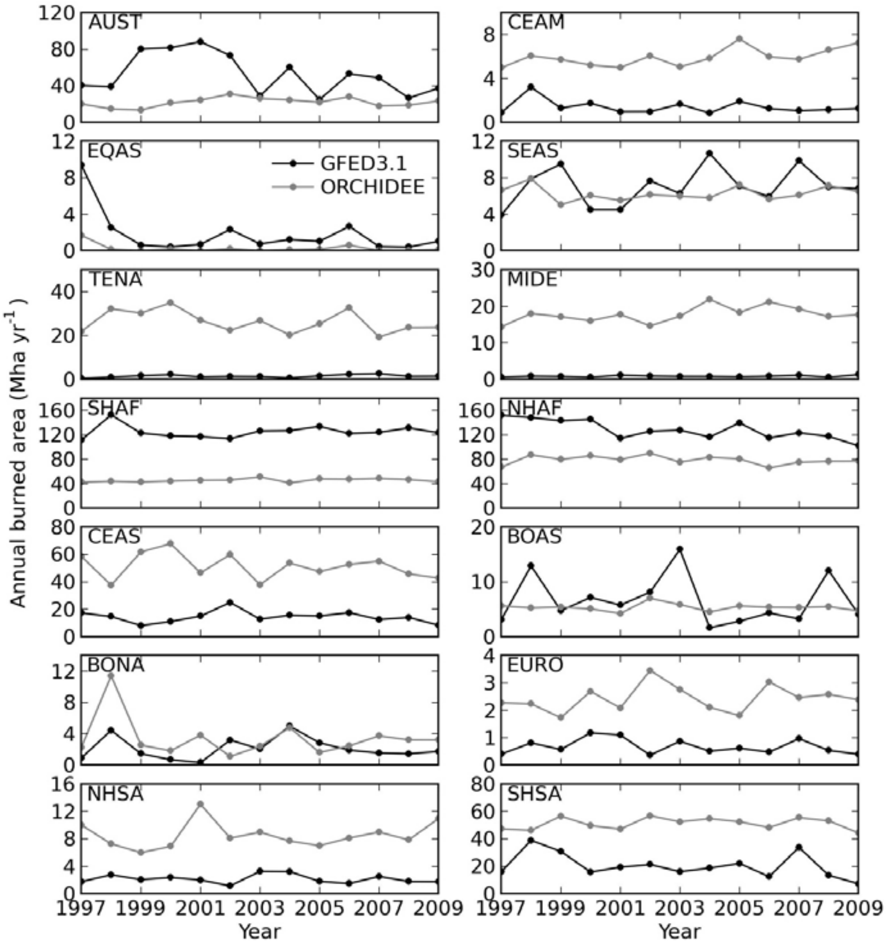

Fig. S4 Annual burned area by ORCHIDEE simulation (grey) and GFED3.1 data (black) for 1997–2009 for the 14 GFED3.1 regions.

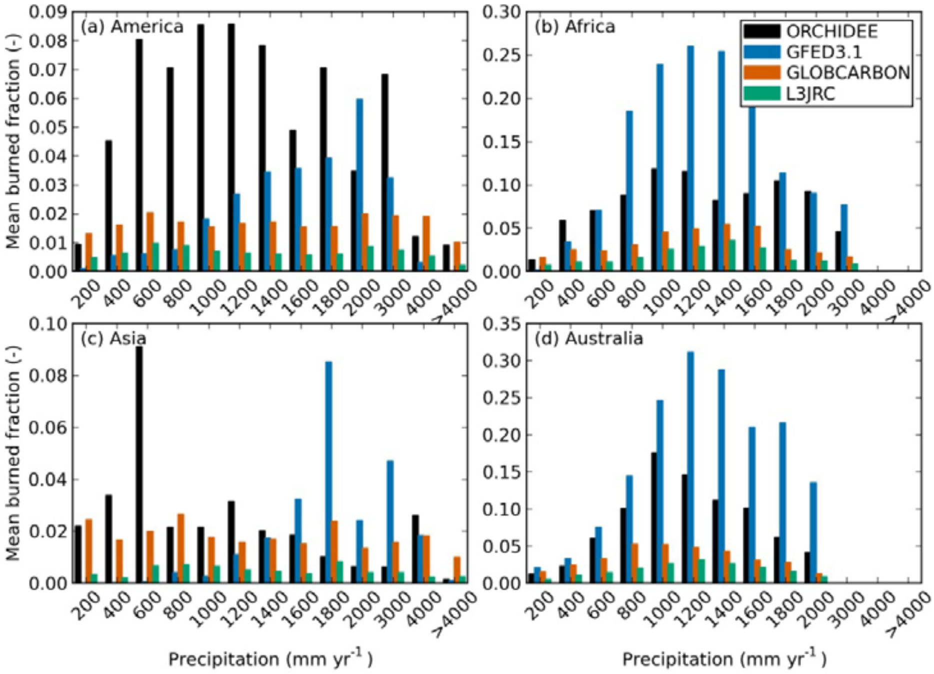

Fig. S5 Burned fraction distribution as a function of annual precipitation according to the model simulation (black), GFED3.1 (blue), GLOBCARBON (orange) and L3JRC (green) datasets for four sub-regions in the tropics and subtropics (S35-N35): (a) America; (b) Africa; (c) Asia; (d) Australia. The annual precipitation data are from CRU data and binned in 200-mm intervals.

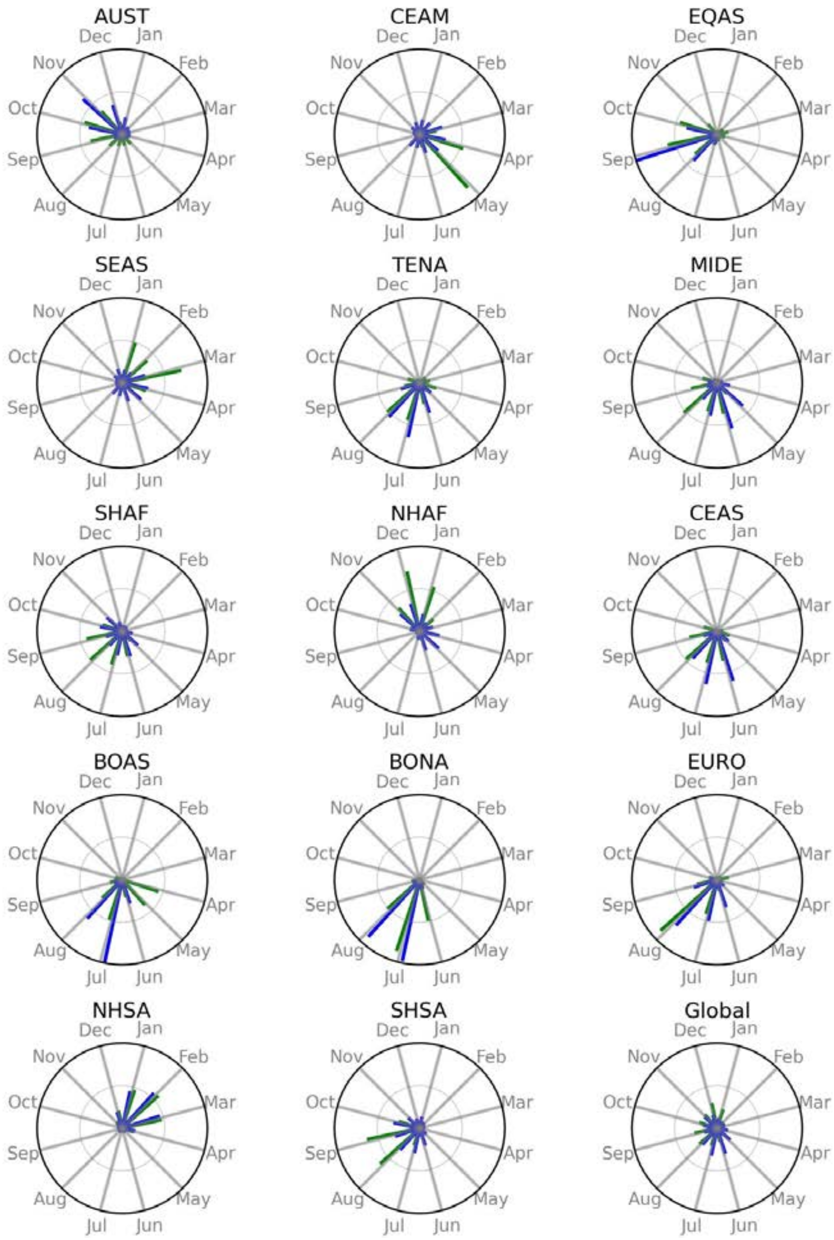

Fig. S6 Normalized monthly burned area for GFED3.1 data (green) and ORCHIDEE simulation (blue) for the globe and the different GFED3.1 regions (see Fig. 2a). The mean monthly burned areas over 1997–2009 are normalized by the annual total of each dataset and the outset black ring represents 0.5 of the annual burned area.

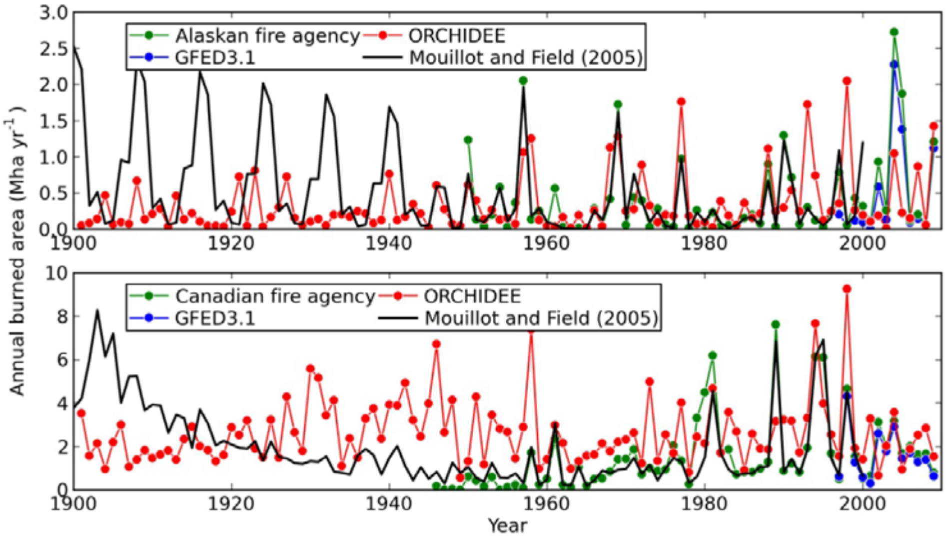

Fig. S7 Historical burned area in Alaska (upper panel) and Canada (lower panel) as simulated by ORCHIDEE (red), and as reported by Mouillot and Field, (2005) (black), government fire agency survey data (green), and GFED3.1 data (blue). The model simulation, the Mouillot data (Mouillot and Field, 2005) and the fire agency survey data agree well with each other for the period for which the statistical data are available. When time goes back to prior to 1950 the model simulation and the Mouillot data begin to diverge, probably because of the decreased reliability in the Mouillot data.

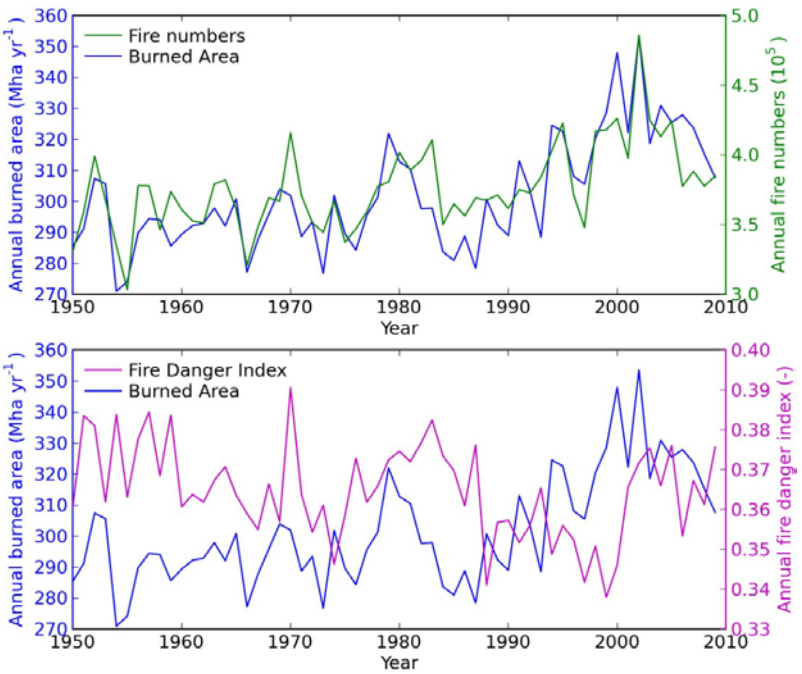

Fig. S8 The major driving factors for the global total burned area for 1950–2009. Upper panel shows the time series of global burned area (blue, left vertical axis) and the global total fire numbers (green, right vertical axis). Lower panel shows the time series of global total burned area (blue, left vertical axis) and the fire danger index (magenta, right vertical axis) as weighted by the burned area.

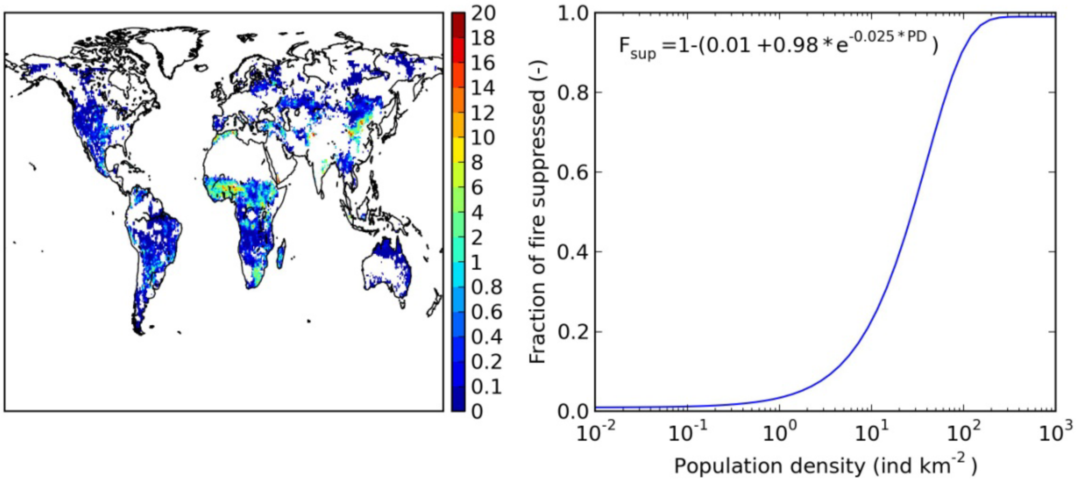

Fig. S9 The influence of applying the effect of human suppression on lightning-caused fires in the model. The left panel shows the mean annual burned fraction reduction due to the human suppression of lightning fires for 1997–2009. The right panel shows the fraction of suppressed lightning ignitions as a function of population density, following Li et al. (2012).

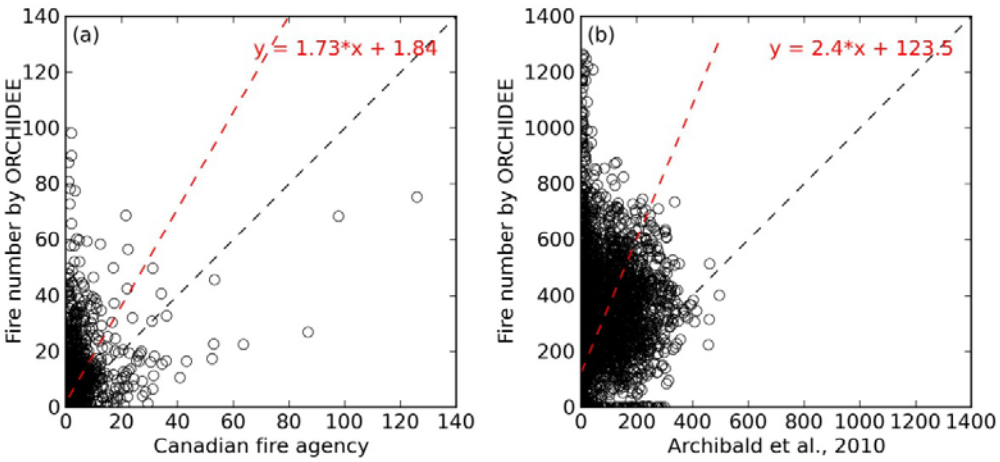

Fig. S10 Pixel-to-pixel comparison of simulated fire number to (a) the fire number reported by Canadian fire agency over 2001-2009, and (b) the fire patch number reported by Archibald et al. (2010) over 2001-2007 for southern Africa by reclassifying the MODIS 500-m burned area data. The red dashed lines show the regression results by the Reduced Major Axis (RMA) linear regression with the regression equations being shown as well. The number of fires for all the datasets is the mean annual fire number based on 0.5^o spatial resolution with each circle in the figure representing a 0.5^o grid cell.

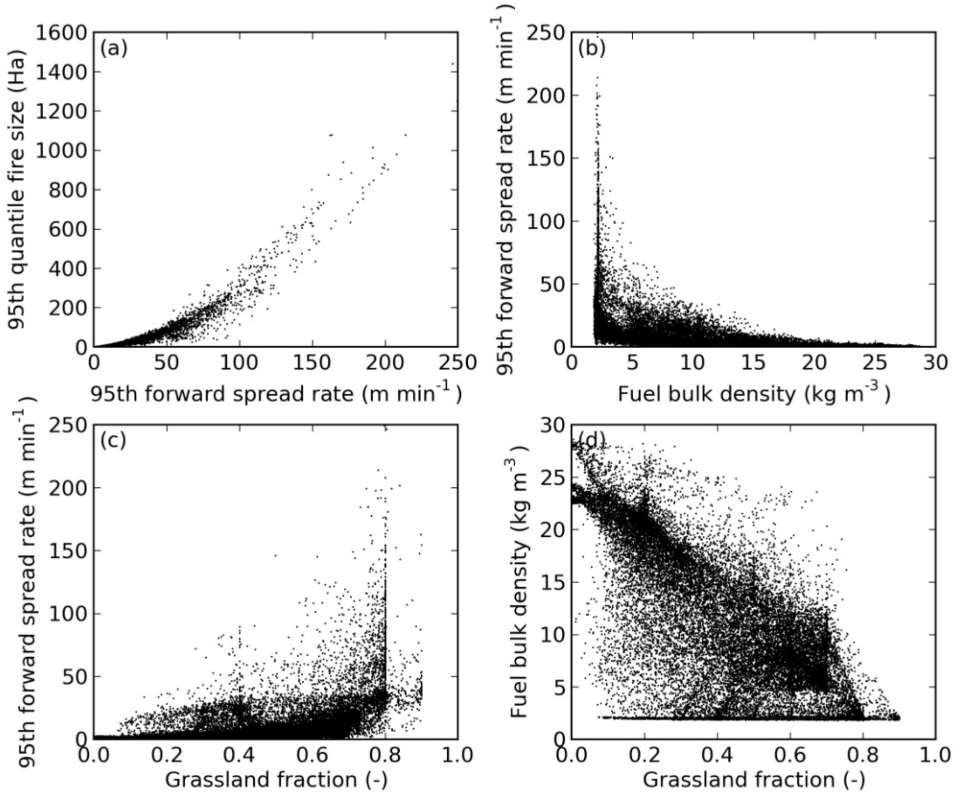

Fig. S11 Factors that influence the simulated fire size: (a) the large fire size (the 95th quantile fire size) is exponentially dependent on the 95th quantile fire forward-spread rate; (b) the 95th quantile fire forward-spread rate is inversely related to the fuel bulk density; (c) the 95th fire forward-spread rate is positively dependent on the grassland fraction (notice the threshold effect around grass fraction of ~0.7); (d) fuel bulk density is inversely related to the grass fraction. All data shown here are for 1997–2009 over the globe and each dot in the figure represents a 0.5^o grid cell.

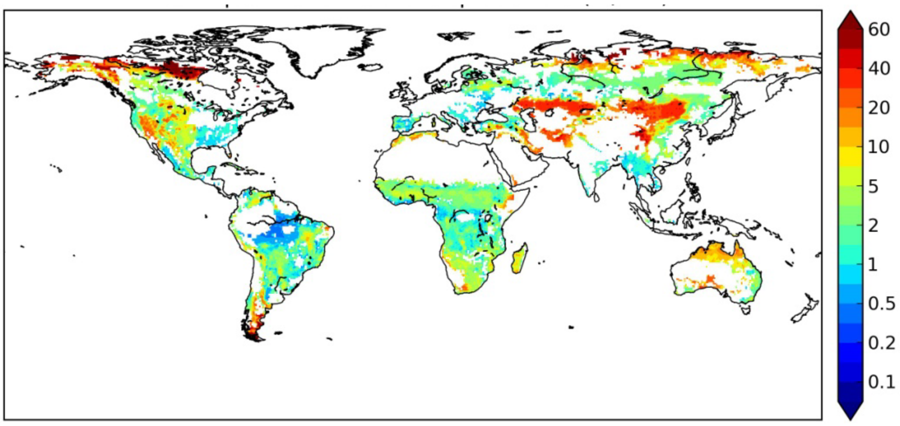

Fig. S12 Map of the 95th quantile fire forward-spread rate (m min^{-1}) as simulated by ORCHIDEE.

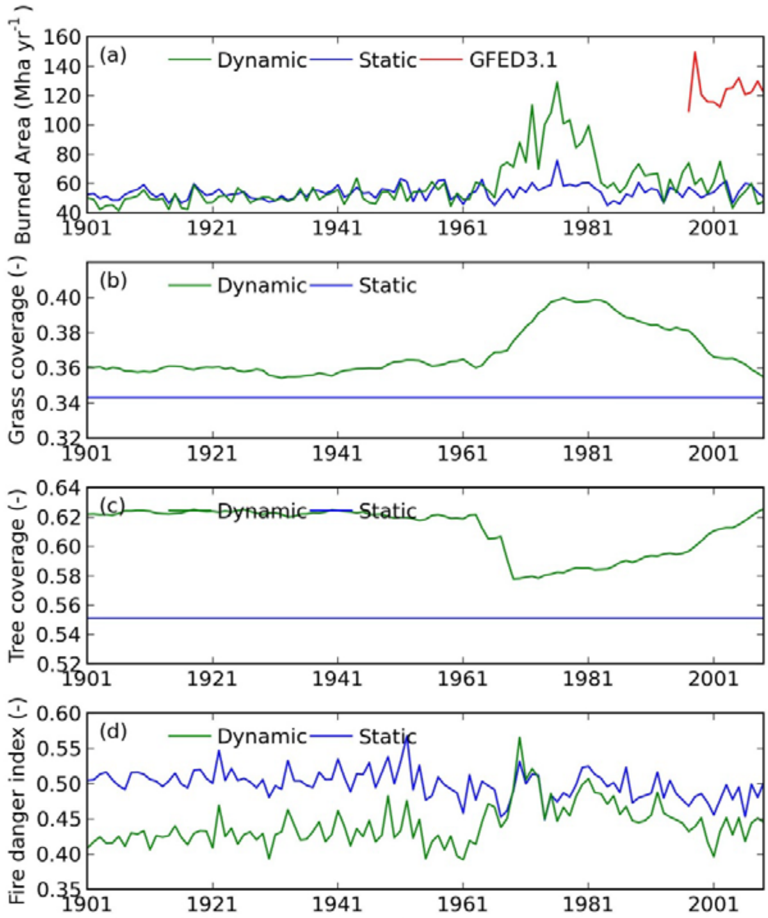

Fig. S13 Comparison of the results for simulations with the dynamic vegetation module of ORCHIDEE being switched on (green, Dynamic vegetation) and off (blue, Static vegetation) for 1901–2009: (a) simulated fire-burned area for dynamic (green) and static (blue) vegetation being compared with GFED3.1 (red) data; (b) simulated mean grass coverage change; (c) simulated tree coverage change; (d) simulated fire danger index as weighted by the burned area. The test simulation was done for southern hemisphere Africa following the same simulation protocol as described in the main text Sect. 2.3 using a slightly different PFT map by Poulter et al. (2011).

Table S1 Mean annual burned area (Mha yr^{-1}) for 2001–2006 for different ORCHIDEE simulation quality flags as shown in main text Fig. 4. The ORCHIDEE result is from the simulation with spatial dataset of a(ND) values (Fig. S1) used in the human ignition equation.

	ORCHIDEE	GFED3.1	GLOBCARBON	L3JRC
ORC-err-burn	29	-	-	-
ORC-err-noburn	-	27	57	92
ORC-good	93	135	73	96
ORC-max	194	31	23	30
ORC-min	30	150	135	167
Global (Total)	347	344	287	384

References:

Archibald, S., Scholes, R. J., Roy, D. P., Roberts, G. and Boschetti, L.: Southern African fire regimes as revealed by remote sensing, Int. J. Wildland Fire, 19(7), 861–878, 2010.

Li, F., Zeng, X. D. and Levis, S.: A process-based fire parameterization of intermediate complexity in a Dynamic Global Vegetation Model, Biogeosciences, 9(7), 2761–2780, doi:10.5194/bg-9-2761-2012, 2012.

Mouillot, F. and Field, C. B.: Fire history and the global carbon budget: a 1 degrees x 1 degrees fire history reconstruction for the 20th century, Global Change Biology, 11, 398–420, doi:10.1111/j.1365-2486.2005.00920.x, 2005.

Poulter, B., Ciais, P., Hodson, E., Lischke, H., Maignan, F., Plummer, S. and Zimmermann, N. E.: Plant functional type mapping for earth system models, Geoscientific Model Development, 4(4), 993–1010, doi:10.5194/gmd-4-993-2011, 2011.

Thonicke, K., Spessa, A., Prentice, I. C., Harrison, S. P., Dong, L. and Carmona-Moreno, C.: The influence of vegetation, fire spread and fire behaviour on biomass burning and trace gas emissions: results from a process-based model, Biogeosciences, 7(6), 1991–2011, 2010.